Petrography of refractory inclusions in CM2.6 QUE 97990 and the origin of melilite-free spinel inclusions in CM chondrites

Alan E. RUBIN

Institute of Geophysics and Planetary Physics, University of California, Los Angeles, California 90095–1567, USA

E-mail: aerubin@ucla.edu

Abstract–Queen Alexandra Range (QUE) 97990 (CM2.6) is among the least-altered CM chondrites known. It contains 1.8 vol% refractory inclusions; 40 were studied from a single thin section. Inclusion varieties include simple, banded and nodular structures as well as simple and complex distended objects. The inclusions range in mean size from 30 to 530 μm and average 130 ± 90 μm. Many inclusions contain 25 ± 15 vol% phyllosilicate (predominantly Mg-Fe serpentine); several contain small grains of perovskite. In addition to phyllosilicate, the most abundant inclusions in QUE 97990 consist mainly of spinel-pyroxene (35%), followed by spinel (20%), spinel-pyroxene-olivine (18%), pyroxene (12%), pyroxene-olivine (8%) and hibonite $\pm$ spinel (8%). Four pyroxene phases occur: diopside, Al-rich diopside (with ≥ 8.0 wt% Al_2O_3), Al-Ti diopside (i.e., fassaite), and (in two inclusions) enstatite. No inclusions contain melilite. Aqueous alteration of refractory inclusions transforms some phases (particularly melilite) into phyllosilicate; some inclusions broke apart during alteration. Melilite-free, phyllosilicate-bearing, spinel inclusions probably formed from pristine, phyllosilicate-free inclusions containing both melilite and spinel. Sixty-five percent of the refractory inclusions in QUE 97990 appear to be largely intact; the major exception is the group of spinel inclusions, all of which are fragments. Whereas QUE 97990 contains about 50 largely intact refractory inclusions/cm^2, estimates from literature data imply that more-altered CM chondrites have lower modal abundances (and lower number densities) of refractory inclusions: Mighei (CM ~ 2.3) contains roughly 0.3–0.6 vol% inclusions (~10 largely intact inclusions/cm^2); Cold Bokkeveld (CM2.2) contains ~0.01 vol% inclusions (on the order of 6 largely intact inclusions/cm^2).

INTRODUCTION

Melilite, a solid solution of åkermanite ($Ca_2MgSi_2O_7$) and gehlenite ($Ca_2Al(Si,Al)_2O_7$), is a common constituent of refractory inclusions in the most primitive carbonaceous chondrites. Fifty percent of the refractory inclusions in CR2 chondrites (Weber and Bischoff 1997) and 45%–74% of those in the least-altered (type 3.0) CO chondrites (Kojima et al. 1995; Russell et al. 1998) are melilite-rich. Acfer 094 is a CM-related, type 3.0 carbonaceous chondrite that has experienced negligible thermal metamorphism (e.g., Kunihiro et al. 2005; Newton et al. 1995). The most abundant phases in refractory inclusions in Acfer 094 are melilite and spinel (Weber 1995). Rubin and Kallemeyn (1990) described two refractory inclusions in the type 3.0–3.1 ungrouped carbonaceous chondrite Lewis Cliff (LEW) 85332; both inclusions are melilite-rich. Refractory inclusions in the reduced CV3 chondrite Vigarano contain unaltered melilite (MacPherson and Grossman 1984).

Although common in unaltered members of other carbonaceous chondrite groups, melilite-rich refractory inclusions are very rare in CM2 chondrites (Fuchs et al. 1973; MacDougall 1979, 1981; Armstrong et al. 1982; MacPherson et al. 1983; Greenwood et al. 1994; MacPherson and Davis 1994). This observation has led several workers to suggest that CM refractory inclusions never contained appreciable amounts of melilite (e.g., MacPherson and Davis 1994; Beckett and Stolper 1994; MacPherson and Huss 2005; Simon et al. 2006).

However, CM chondrites have undergone extensive pre-terrestrial aqueous alteration, and it seems possible that such parent-body processes destroyed pre-existing melilite in CM refractory inclusions. CM chondrites contain appreciable amounts of phyllosilicate (Barber 1981, 1985; Tomeoka and Buseck 1985); also present in CM-chondrite matrices are clumps of serpentine-tochilinite intergrowths (formerly called "poorly characterized phases," or PCP), pentlandite, and Ni-bearing pyrrhotite. Several authors have noted that different

CM chondrites vary in their degree of aqueous alteration (McSween 1979; Browning et al. 1996; Hanowski and Brearley 2001; Rubin et al. 2007). Because Armstrong et al. (1982) suggested that parent-body alteration processes may have destroyed primary melilite in CM refractory inclusions, it seemed worthwhile to investigate refractory inclusions in minimally altered CM chondrites.

Rubin et al. (2007) identified Queen Alexandra Range (QUE) 97990 as the least-altered CM chondrite. The rock contains ~1 vol% metallic Fe-Ni compared to 0.27 vol% in Yamato (Y-) 791198, 0.16 vol% in Murray, 0.11 vol% in Murchison, and 0.09 vol% in Nogoya (Rubin et al. 2007). Although the glassy mesostases of chondrules in QUE 97990 have been altered to hydrated phases, mafic-silicate phenocrysts in the chondrules appear unaffected. In contrast, olivine and pyroxene within the vast majority of chondrules in more-altered CM2 chondrites such as QUE 93005 have been transformed into phyllosilicates. QUE 97990 thus offers the best opportunity to study minimally altered CM refractory inclusions.

ANALYTICAL PROCEDURES

A previously prepared mosaic of high-resolution (2 μm/pixel) backscattered electron (BSE) images of thin section QUE 97990,13 was studied. The BSE images were made with the LEO 1430 VP scanning electron microscope (SEM) at UCLA using a 15 keV accelerating voltage and a working distance of ~19 mm. A grid divided into square-millimeter sections was superimposed on the BSE mosaic to allow rapid determination of component coordinates. The abscissa was labelled alphabetically, the ordinate numerically; each millimeter square was divided into a 5×5 matrix and each 200 μm square was labelled alphabetically. The label of each refractory inclusion was assigned based on its location in the matrix. A 10-element X-ray map covering a rectangular area of ~50 mm^2 of the thin section was made using the JEOL JXA-8200 electron microprobe at UCLA. An RGB map (red = Mg, green = Ca, blue = Al) was constructed from the X-ray maps and used to identify Ca- and Al-rich inclusions. Previously prepared 10-element X-ray maps and BSE images of two different 1 mm^2 portions of single thin sections of seven other CM chondrites were also examined in a search for refractory inclusions: Cold Bokkeveld (USNM 182-2); La Paz Ice Field (LAP) 02277,10; Meteorite Hills (MET) 01070,7; Murchison (USNM 5376-5); QUE 93005,9; QUE 99355,6; and Y-791198,90-1. The Cold Bokkeveld and Murchison sections are from the Smithsonian Institution, the QUE, LAP, and MET sections are from NASA Johnson Space Center, and the Y-791198 section is from the National Institute of Polar Research in Japan.

BSE images of individual inclusions were made with the LEO 1430 SEM; inclusion and grain sizes were measured on the BSE images using the automated scale. Mineral compositions were determined with a focused beam using the JEOL electron microprobe, employing natural and synthetic standards, an accelerating voltage of 15 keV, a 15 nA sample current, 20 s counting times per element, and ZAF corrections. Under these operating conditions, the detection limit is ~0.05 wt%.

RESULTS

Petrography

Forty refractory inclusions were found in the analyzed ~50 mm^2 area of thin section QUE 97990,13 (Table 1). They range in mean size from ~30 to 530 μm and average 130 ± 90 μm. (The mean size is the average of the longest dimension c and the longest dimension perpendicular to c.) The inclusions constitute 1.8 vol% of the meteorite. Small grains of perovskite are present in several inclusions. Many inclusions contain 25 ± 15 vol% phyllosilicate; it is difficult to determine which phase or phases the phyllosilicate is replacing. The most abundant inclusions in QUE 97990 consist (in addition to phyllosilicate) primarily of spinel-pyroxene, followed by those consisting mainly of spinel, spinel-pyroxene-olivine, pyroxene, pyroxene-olivine, and hibonite ± spinel. Four pyroxene phases occur in the QUE 97990 inclusions (Table 2): diopside, Al-rich diopside (with ≥8.0 wt% Al$_2$O$_3$), Al-Ti diopside (i.e., fassaite), and, in two inclusions, enstatite. No inclusions contain melilite. Sixty-five percent of the inclusions appear to be largely intact; the major exception is the group of spinel inclusions, all of which are fragments. (Objects are considered fragments if they are disjointed or appear likely to consist of <50% of the original object.)

I have made modifications in the definitions and labels of the structural types of CM refractory inclusions used by MacPherson and Davis (1994):

- Simple inclusions are relatively coherent objects that do not appear to have been stretched out.
- Nodular inclusions are composed of rounded or botryoidal nodules; in most cases, the nodules consist of spinel cores rimmed by pyroxene.
- Banded inclusions contain elongated continuous or discontinuous ribbons of a primary phase; in many inclusions there are spinel ribbons rimmed by pyroxene. There is a continuum between nodular and banded inclusions; simple inclusions can include both varieties.
- Simple distended inclusions are elongated variegated objects containing isolated single crystals and grain clusters, and, in some cases, also containing sinuous chains of grains (in most of these cases, spinel).
- Complex distended inclusions consist of several disjointed portions enclosed by a common rim of pyroxene and/or a mantle of phyllosilicate. The refractory inclusions in QUE 97990 include simple, banded, and nodular structures as well as simple and complex distended inclusions.

Table 1. Refractory inclusions from thin section QUE 97990,13.

Inclusion	Size (μm)	Primary structure	Condition
Spinel-pyroxene inclusions (14/40)			
E1n	41 × 79	Banded	Fragment
E2u	56 × 104	Nodular	Largely intact
G4m	104 × 212	Complex distended incl	Largely intact
E3s	131 × 253	Banded	Largely intact
G6v	118 × 154	Banded	Largely intact
H8y	83 × 115	Banded; simple incl	Largely intact
H8r	52 × 76	Complex distended incl	Largely intact
F7o	159 × 204	Complex distended incl	Largely intact
C6v	85 × 336	Simple distended	Largely intact
C6q	100 × 104	Banded	Fragment
F8y	47 × 158	Simple distended incl	Fragment
E8y	37 × 51	Banded	Largely intact
F10a	64 × 121	Banded	Largely intact
K4u	136 × 141	Banded	Largely intact
Spinel inclusions (8/40)			
H6k	84 × 133	Complex distended incl	Fragment
E6d	33 × 58	Simple distended incl	Fragment
E7m	36 × 103	Banded	Fragment
E6p	31 × 35	Simple distended incl	Fragment
E8j	61 × 85	Nodular	Fragment
G7n	40 × 55	Simple distended incl	Fragment
H8x	140 × 232	Complex distended incl	Fragment
H8s	46 × 48	Simple distended incl	Fragment
Spinel-pyroxene-olivine inclusions (7/40)			
J5g	388 × 662	Simple incl	Largely intact
G3s	154 × 172	Nodular	Largely intact
F2x	92 × 135	Nodular	Largely intact
C7u	66 × 97	Banded	Largely intact
D10y	310 × 353	Nodular	Largely intact
H1r	61 × 100	Nodular	Largely intact
G10t	112 × 155	Nodular	Largely intact
Pyroxene inclusions (5/40)			
E2w	80 × 124	Simple incl	Largely intact
H6q	60 × 130	Simple incl	Largely intact
H6u	171 × 385	Simple incl	Largely intact
F9m	127 × 194	Simple incl	Largely intact
B7f	174 × 315	Simple incl	Largely intact
Pyroxene-olivine inclusions (3/40)			
G7x	96 × 268	Complex distended incl	Fragment
C5f	48 × 93	Banded	Fragment
G10y	94 × 157	Banded	Largely intact
Hibonite-bearing inclusions (3/40)			
F3r	82 × 172	Complex distended inclusion	Largely intact
C7y	43 × 68	Simple inclusion	Largely intact
H8t	27 × 42	Simple distended inclusion	Fragment

Spinel-Pyroxene Inclusions

Spinel-pyroxene inclusions (Figs. 1a–c) constitute 14 of the 40 studied inclusions (35%). They range from 37×51 μm to 85×336 μm and have a mean size of 120 ± 50 μm. Eight of the inclusions have banded structures, one is nodular, two are simple distended inclusions, and three are complex distended inclusions. Eleven of the inclusions appear to be largely intact; three are fragments. On average, they contain 20 ± 14 vol% phyllosilicate.

Most banded inclusions consist of a rim of diopside 3–10 μm thick surrounding a core of spinel grains ~3–40 μm in size (e.g., Figs. 1a and 1b). In one inclusion (G6v), there is an

Table 2. Mean compositions and standard deviations (wt%) of pyroxene phases in refractory inclusions in QUE 97990.

	Spinel-pyroxene inclusions				Spinel-pyroxene-olivine inclusions			
	Diopside	Al-rich diopside	Al-Ti diopside	Enstatite	Diopside	Al-rich diopside	Al-Ti diopside	Enstatite
No. points	27	17	5	2	18	9	4	1
SiO_2	51.7 ± 2.1	47.0 ± 3.6	32.4 ± 4.3	57.4 ± 0.3	52.6 ± 1.2	48.5 ± 0.6	36.4 ± 2.9	58.7
TiO_2	0.67 ± 0.88	1.7 ± 0.7	12.2 ± 4.7	0.84 ± 0.36	0.41 ± 0.32	1.3 ± 0.8	7.6 ± 0.3	0.22
Al_2O_3	3.6 ± 1.3	11.1 ± 4.9	23.1 ± 2.6	1.1 ± 0.1	3.9 ± 1.8	9.6 ±1.3	21.7 ± 3.1	1.4
Cr_2O_3	0.17 ± 0.16	0.18 ± 0.24	0.12 ± 0.01	0.72 ± 0.19	<0.05	0.06 ± 0.04	0.13 ± 0.08	0.57
FeO	1.6 ± 1.3	0.86 ± 0.51	0.66 ± 0.43	1.1 ± 0.2	0.37 ± 0.16	0.37 ± 0.10	0.42 ± 0.11	0.66
MnO	0.06 ± 0.08	<0.05	<0.05	0.25 ± 0.00	<0.05	<0.05	<0.05	0.10
MgO	18.4 ± 1.4	15.1 ± 1.2	7.5 ± 3.1	36.7 ± 0.0	17.9 ± 0.9	15.4 ± 0.7	10.5 ± 1.6	38.5
CaO	23.4 ± 1.9	24.5 ± 1.2	24.0 ± 0.6	2.5 ± 0.1	25.1 ± 0.6	24.9 ± 0.8	23.7 ± 1.6	0.44
Total	99.6	100.4	100.0	100.6	100.3	100.1	100.4	100.6
mol% Fs	2.6 ± 2.0	1.6 ± 1.0	1.5 ± 1.1	1.5 ± 0.3	0.58 ± 0.24	0.61 ± 0.17	0.86 ± 0.23	0.94
mol% Wo	46.6 ± 3.4	53.2 ± 1.5	69.2 ± 8.5	4.6 ± 0.3	50.0 ± 1.6	53.5 ± 1.8	61.3 ± 4.9	0.80

Table 2. *Continued.* Mean compositions and standard deviations (wt%) of pyroxene phases in refractory inclusions in QUE 97990.

	Pyroxene inclusions			Pyroxene-olivine inclusions		
	Diopside	Al-rich diopside	Al-Ti diopside	Diopside	Al-rich diopside	Al-Ti diopside
No. points	14	5	1	6	6	1
SiO_2	53.4 ± 0.6	47.6 ± 2.7	36.5	52.5 ± 1.4	47.7 ± 1.5	32.3
TiO_2	0.43 ± 0.37	0.77 ± 0.19	10.5	0.39 ± 0.27	1.3 ± 0.3	11.8
Al_2O_3	2.8 ± 1.3	10.1 ± 4.0	19.0	3.3 ± 2.0	8.5 ± 2.5	23.3
Cr_2O_3	0.16 ± 0.23	0.06 ± 0.07	0.17	<0.05	0.11 ± 0.08	0.09
FeO	0.95 ± 0.52	1.5 ± 0.6	0.65	0.76 ± 0.10	2.1 ± 2.5	0.41
MnO	0.06 ± 0.08	<0.05	<0.05	<0.05	<0.05	<0.05
MgO	19.1 ± 2.0	15.7 ± 0.5	9.8	19.2 ± 2.2	16.1 ± 0.4	7.1
CaO	23.8 ± 3.2	24.0 ± 1.1	24.0	24.1 ± 0.7	23.2 ± 1.2	23.7
Total	100.7	99.7	100.6	100.2	99.0	98.7
mol% Fs	1.5 ± 0.8	2.4 ± 1.0	1.3	1.2 ± 0.2	3.5 ± 4.0	0.95
mol% Wo	46.5 ± 6.2	51.1 ± 1.4		46.9 ± 3.5	49.1 ± 3.6	69.9

inner layer of Al-Ti diopside 2–7 μm thick between the diopside rim and the spinel core. Al-rich diopside (with ≥8.0 wt% Al_2O_3) occurs in a few inclusions, either as the primary rim (inclusions C6q and K4u) or as small (2–4 μm in size) patches within the diopside rim. Spinel is only a minor to accessory phase in three inclusions (E3s, H8y, C6q), where it occurs as widely separated ~2 μm grains. In inclusion K4u, the Al-diopside rim is invaginated, folding in toward the center of the inclusion. Many of the inclusions contain small patches of phyllosilicate adjacent to spinel grains in the core.

Inclusions C6v (Fig. 1c) and F8y are simple distended inclusions. They consist of isolated patches of spinel grains 5–25 μm in size rimmed by mantles of diopside ~2 μm thick (inclusion C6v) or Al-rich diopside (F8y). There is a grain of enstatite 7 μm in size adjacent to spinel near the edge of inclusion C6v (Fig. 1c). Phyllosilicate occurs around the rimmed spinel grains; the phyllosilicate is difficult to distinguish from the fine-grained matrix material in the meteorite.

Inclusion G4m is a complex distended inclusion consisting of clusters of spinel cores 5–10 μm in size

surrounded by 2 μm thick rims composed of diopside and Al-rich diopside. These clusters occur mainly along the edge of the inclusion. The other two complex distended inclusions (H8r, F7o) consist of spinel grains 3–4 μm in size surrounded by 3 μm thick rims of diopside (F7o) or Al-rich diopside (H8r). All of the inclusions contain central patches dominated by phyllosilicate.

Nodular inclusion E2u (Fig. 1a) appears to consist of connected banded inclusions. Each portion contains a core of spinel 3–25 μm in size surrounded by 3–7 μm thick rims of Al-rich diopside.

Spinel-Pyroxene-Olivine Inclusions

Spinel-pyroxene-olivine inclusions (Fig. 1d–f) constitute 7 of the 40 inclusions (18%). They range from 61 × 100 μm to 388 × 662 μm and have a mean size of 200 ± 170 μm. One inclusion has a banded structure, five are nodular, and one inclusion has a "simple" structure consisting of intergrown phases. All of the inclusions appear to be largely intact. They contain the lowest phyllosilicate abundances (5 ± 3 vol%) of any inclusion type.
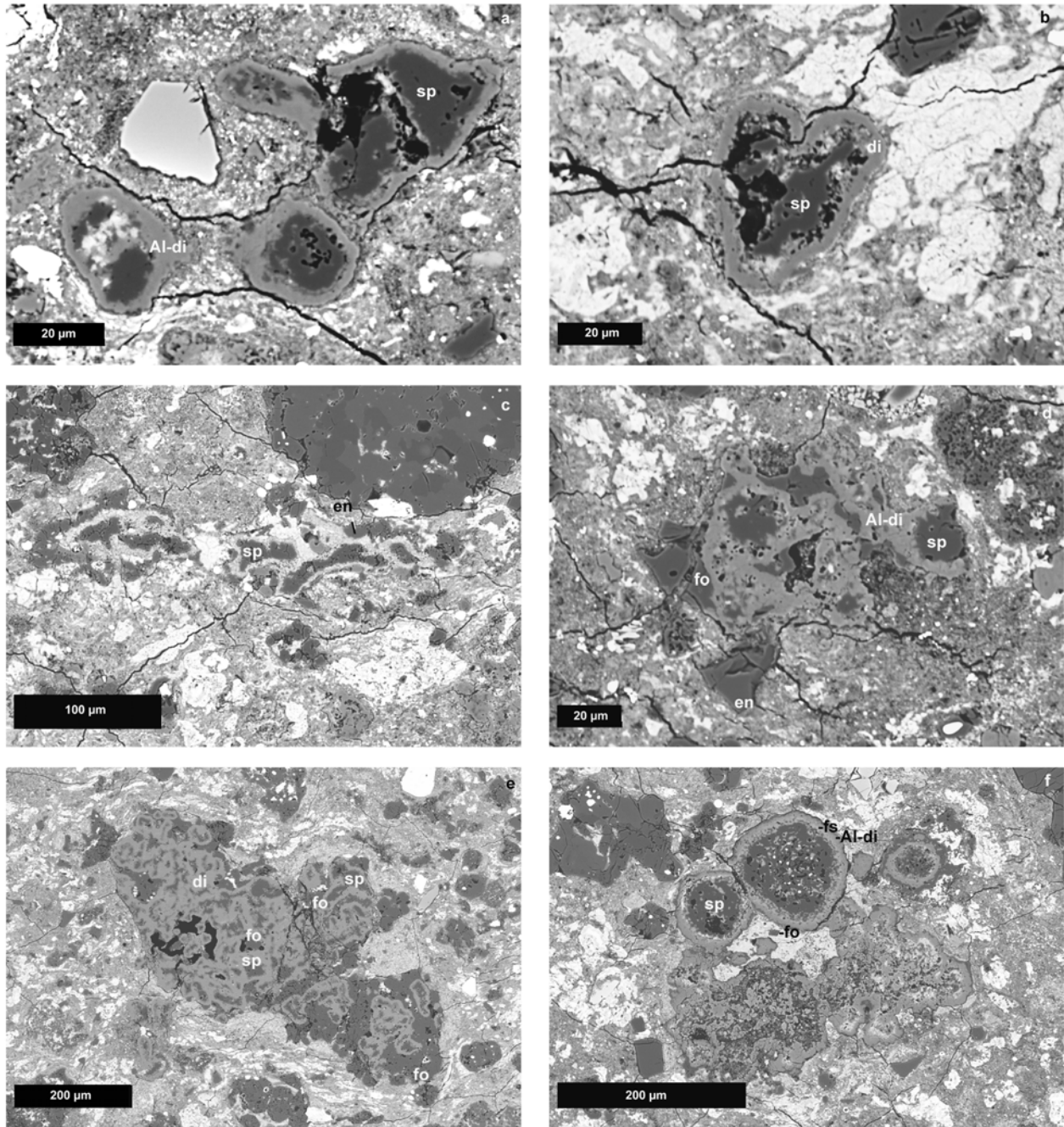
Fig. 1. Spinel-pyroxene and spinel-pyroxene-olivine inclusions. a) Spinel-pyroxene inclusion E2u has a nodular structure and consists of connected banded inclusions, each composed of a spinel core (dark gray) surrounded by a rim of Al-rich diopside (light gray). Black areas are plucked regions. b) Spinel-pyroxene inclusion E8y has a banded structure consisting of a spinel core (dark gray) surrounded by a heart-shaped rim of diopside (light gray). Black areas are plucked regions. c) Spinel-pyroxene inclusion C6v is a simple distended inclusion consisting of clusters of spinel grains (dark gray) rimmed by thin mantles of diopside (light gray). A grain of enstatite 7 μm in size is adjacent to spinel near the edge of the inclusion. Also present throughout the inclusion are patches of phyllosilicate (light gray, mottled) that probably formed by alteration on the parent body. d) Spinel-pyroxene-olivine inclusion H1r has a nodular structure and consists of spinel grains (dark gray) surrounded by bands of Al-rich diopside. Also present in the inclusion are grains of forsterite (fo) and enstatite (en). e) Spinel-pyroxene-olivine inclusion J5g, the largest inclusion in the set, is a simple inclusion consisting of evenly dispersed patches of spinel (dark gray) and forsterite (dark gray) surrounded by diopside (light gray). Black areas are plucked regions. f) Spinel-pyroxene-olivine inclusion D10y is a multi-lobate object composed of rounded nodules, each consisting of a spinel core (dark gray) surrounded by rims of Al-rich diopside 10 μm thick. There is an inner rim composed of Al-Ti diopside (fassaite) (light gray). Several small grains of perovskite (white) occur within some of the spinel cores. Small grains of Al-Ti diopside and forsterite are present in irregularly shaped nodules on the other side of the inclusion. sp = spinel; di = diopside; Al-di = Al-rich diopside; en = enstatite; fs = fassaite (i.e., Al-Ti diopside); fo = forsterite.
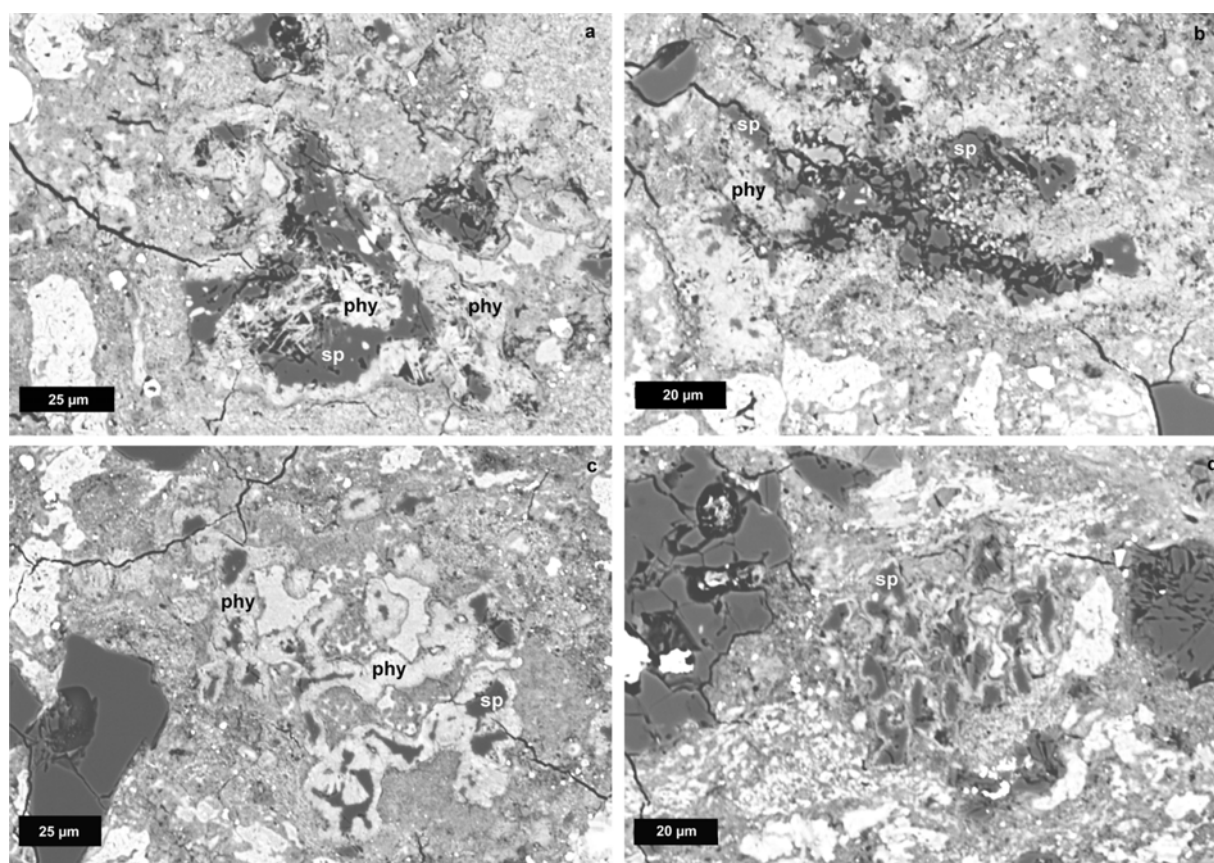
Fig. 2. Spinel inclusion fragments. a) Nodular inclusion E8j consists of a massive spinel core (dark gray) surrounded by a phyllosilicate mantle (light gray). b) Banded inclusion E7m contains continuous ribbons of spinel (dark gray) mantled by phyllosilicate (light gray). Also present are small grains of perovskite (white). Black areas are plucked regions. c) Inclusion H6k is a complex distended inclusion containing patches of spinel (dark gray) surrounded by phyllosilicate (light gray). d) Inclusion G7n is a simple distended inclusion consisting of small spinel grains (dark gray) surrounded by thin mantles of phyllosilicate (light gray). Most of the spinel grains in this inclusion are elongated; many appear to be subparallel. sp = spinel; phy = phyllosilicate.

The banded inclusion (C7u) consists of elongated spinel grains 3–15 × 5–50 μm in size surrounded by an 8–16 μm thick mantle of Al-rich diopside. Forsterite occurs as grains at the edge of the inclusion 2–10 μm in size.

Nodular inclusions H1r (Fig. 1d) and G10t consist of spinel grains 15 μm in size surrounded by bands of Al-rich diopside. Forsterite occurs as grains at the periphery of the inclusions 10–20 μm in size; in inclusion H1r, enstatite is associated with forsterite. Inclusion D10y (Fig. 1f) is a multi-lobate object composed of several rounded nodules, each consisting of a spinel core surrounded by 10 μm thick rims of Al-rich diopside; in addition, grains of perovskite ~2 μm in size occur within some of the spinel cores. Small grains of Al-Ti diopside and forsterite are present in irregularly shaped nodules on the other side of the inclusion.

The largest inclusion in the present study (inclusion J5g; Fig. 1e) has a simple structure consisting of evenly dispersed, rounded, elongated, and irregularly shaped grains of spinel 14–85 μm in size and rare forsterite surrounded by diopside. The texture resembles that of a cotectic intergrowth of spinel and diopside.

Spinel Inclusions

Spinel inclusions (Figs. 2a–d) constitute 8 of the 40 inclusions (20%). They range from 31 × 35 μm to 140 × 232 μm and have a mean size of 76 ± 50 μm. One inclusion has a banded structure, one is nodular, four are simple distended inclusions, and two are complex distended inclusions. All of the inclusions are fragments. The inclusions typically consist of spinel grains 3–15 μm in size surrounded by rims of phyllosilicate 3–6 μm thick (probably an alteration product of a primary phase). The fibrous texture of the phyllosilicate in inclusion E8j (Fig. 2a) is similar to that observed in some refractory inclusions in CV3 Allende (Ford and Brearley 2007). The mean modal abundance of phyllosilicate is higher in these inclusions (50 ± 20 vol%) than in those from other types of inclusions (5–40 vol%).

Pyroxene Inclusions

Pyroxene inclusions (Figs. 3a and 3b) constitute 5 of the 40 inclusions (12%). They range from 60 × 130 μm to 174 × 315 μm and have a mean size of 180 ± 80 μm. All of the inclusions have a simple structure and consist of intergrown
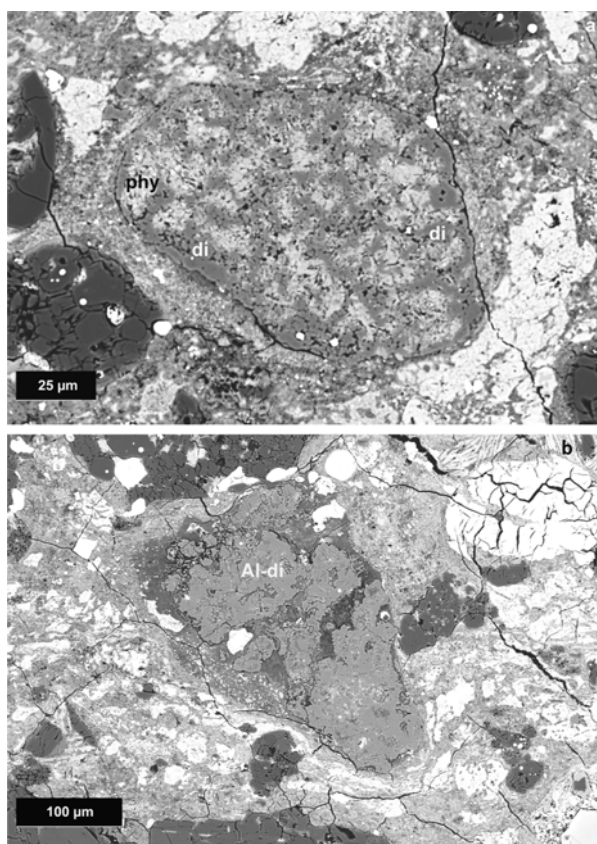
Fig. 3. Pyroxene inclusions. a) Inclusion E2w has a simple structure consisting of intergrown grains of diopside (medium gray). Between the diopside grains are patches of phyllosilicate (light gray). b) Inclusion B7f has a simple structure consisting of massive Al-rich diopside (medium gray). di = diopside; Al-di = Al-rich diopside; phy = phyllosilicate.

Ca-pyroxene grains—diopside in inclusions E2w (Fig. 3a) and H6u, Al-rich diopside in F9m and B7f (Fig. 3b), and diopside plus Al-Ti diopside in H6q. Each inclusion contains patches of phyllosilicate in its core and mantle. All of the inclusions appear to be largely intact. They contain a mean modal abundance of 20 ± 7 vol% phyllosilicate.

Pyroxene-Olivine Inclusions

Pyroxene-olivine inclusions (Figs. 4a and 4b) constitute 3 of the 40 inclusions (8%). They range from 48×93 µm to 96×268 µm and have a mean size of 130 ± 60 µm. Two of the inclusions have banded structures; the other is a complex distended inclusion. One of the banded inclusions (G10y; Fig. 4b) appears to be largely intact; the two remaining inclusions are fragments. The mean modal abundance of phyllosilicate is 30 ± 18 vol%.

The banded inclusions consist of grains of forsterite 4–12 µm in size surrounded by 1–5 µm thick rims or patches of Ca-pyroxene: diopside in C5f (Fig. 4a) and Al-rich diopside plus rare Al-Ti diopside in G10y. Phyllosilicate occurs around the Ca-pyroxene bands. Complex distended inclusion G7x
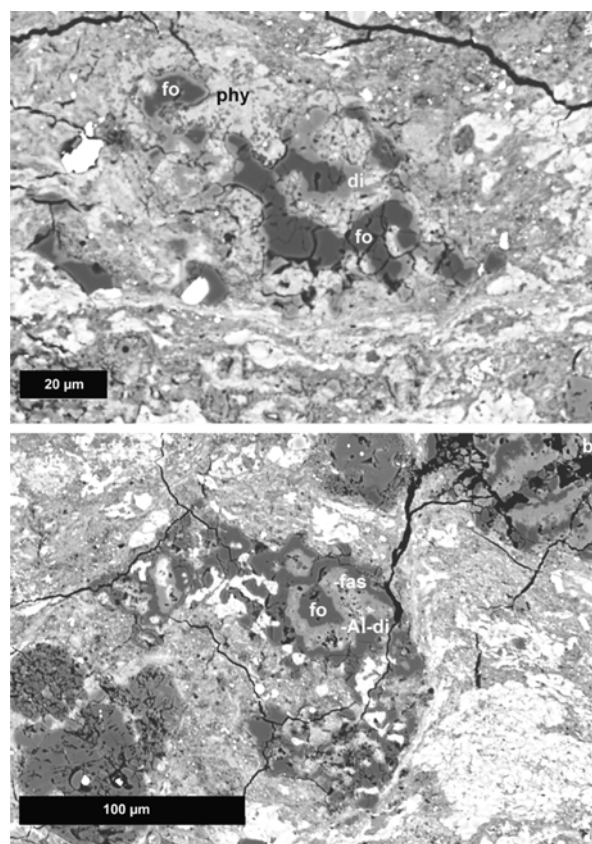

Fig. 4. Pyroxene-olivine inclusions. a) Inclusion C5f is an inclusion fragment with a banded structure. It consists of blocky grains and elongated ribbons of forsterite (dark gray) rimmed by diopside (medium gray). Also present are patches of phyllosilicate (light gray). b) Inclusion G10y has a predominantly banded structure, grading into a nodular structure. The inclusion consists of elongated patches and ribbons of forsterite (dark gray) surrounded by Al-rich diopside (light gray) and rare Al-Ti diopside (very light gray). fo = forsterite; di = diopside; Al-di = Al-rich diopside; fas = fassaite (i.e., Al-Ti diopside); phy = phyllosilicate.

consists of irregular forsterite grains 7–50 µm in size adjacent to patches of diopside 15 µm in size. The entire inclusion is surrounded by a mantle of phyllosilicate.

Hibonite-Bearing Inclusions

Hibonite-bearing inclusions (Figs. 5a and 5b) constitute 3 of the 40 inclusions (8%). They range from 27×42 µm to 82×172 µm and have a mean size of 70 ± 50 µm. One inclusion has a simple structure, one is a simple distended inclusion, and one is a complex distended inclusion. Two of the inclusions (F3r and C7y) appear to be largely intact; inclusion H8t is a fragment. The mean modal abundance of phyllosilicate is 40 ± 31 vol%.

Inclusions F3r (Fig. 5a) and H8t consist of grains of hibonite 5–10 µm in size, some of which enclose subhedral grains of spinel ~5 µm in size. Inclusion C7y (Fig. 5b) consists of anhedral grains and blades of hibonite 10 µm in size and a core made up mainly of phyllosilicate.
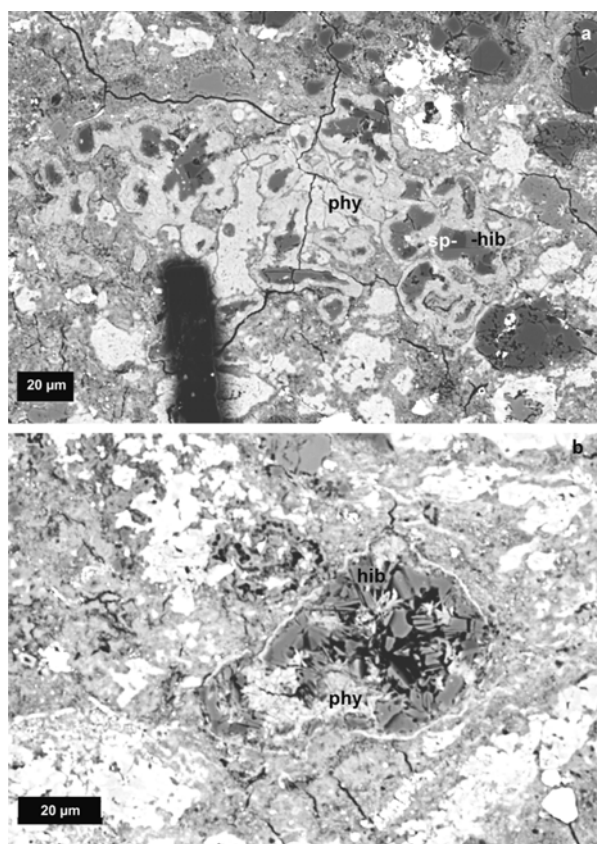
Fig. 5. Hibonite-bearing inclusions. a) Inclusion F3r is a complex distended inclusion consisting of irregularly shaped patches of hibonite (medium-dark gray) surrounded by a mantle of phyllosilicate (light gray). Two distinct varieties of phyllosilicate occur: one is compositionally close to chamosite (darker shade); the other is compositionally close to greenalite (lighter shade). Some of the hibonite grains enclose small subhedral grains of spinel (dark gray). The elongated black object at the bottom of the image is a fiber on the thin section. b) Inclusion C7y has a simple structure consisting of anhedral grains and blades of hibonite (medium gray) and a core made up mainly of phyllosilicate (light gray, bottom left of the inclusion). Black areas are plucked regions. hib = hibonite; sp = spinel; phy = phyllosilicate.

Search for Inclusions in Other CM Chondrites

Refractory inclusions were searched for in the X-ray maps of two 1 mm² portions of thin section Y-791198,90-1. One inclusion was found: a fragment of a spinel inclusion 83×174 μm in size with a banded structure. A patch of phyllosilicate ~10 μm thick occurs between the bands; additional phyllosilicate surrounds one of the spinel bands. The overall phyllosilicate abundance in the inclusion is ~30 vol%. The occurrence of this single inclusion suggests (with high uncertainty) an approximate modal abundance of refractory inclusions in Y-791198 of 0.7 vol%.

No refractory inclusions were identified in the X-ray maps of the two separate 1 mm² portions of the other six CM chondrites in this study: Cold Bokkeveld, LAP 02277, MET 01070, Murchison, QUE 93005, and QUE 99355.

Mineral Compositions

The compositions of the mafic silicate phases (olivine, diopside, Al-rich diopside, Al-Ti diopside) in the QUE 97990 inclusions are very similar to those in other carbonaceous chondrites (Tables A3.19 and A3.22 in Brearley and Jones 1998).

Although oxides in QUE 97990 inclusions are also similar to those in other carbonaceous chondrites, there are some differences in the concentrations of minor elements. For example, hibonite in QUE 97990 inclusions (Table 3) is very similar to that reported from inclusions in Mighei (MacPherson and Davis 1994) and CV3 Allende. However, the FeO content (0.76 wt%) of hibonite in QUE 97990 inclusions is higher than that in inclusions in CM2 Murchison (0.02–0.23 wt%; Table A3.9 in Brearley and Jones 1998). Perovskite in QUE 97990 inclusions tends to be richer in Al_2O_3 (1.7–2.1 wt%), FeO (0.17–1.1 wt%), and MgO (0.56–0.94 wt%) than that in Allende inclusions (0.17–2.0 wt% Al_2O_3; <0.02–0.50 wt% FeO; <0.02–0.23 wt% MgO; Table A3.11 of Brearley and Jones 1998). However, because of the small sizes of the perovskite grains, it is possible that the analyses reflect secondary fluorescence of Al and Mg from the surrounding spinel. Minor elements in spinel in the QUE 97990 inclusions overlap the ranges for other CM chondrites (Table A3.15 in Brearley and Jones 1998).

There are a few slight differences in mineral composition among the different varieties of refractory inclusions in QUE 97990. Diopside in the spinel-pyroxene-olivine inclusions has slightly higher mean CaO (25.1 wt%) and lower mean FeO (0.37 wt%) than diopside in the other inclusion varieties (23.4–24.1 wt% and 0.76–1.6 wt%, respectively) (Table 2).

Spinel in the spinel-pyroxene-olivine inclusions has somewhat lower mean FeO (0.30 wt%) than spinel in the other inclusion varieties (0.82–0.97 wt%) (Table 3). The mean Cr_2O_3 content of spinel in the pyroxene-bearing inclusions is higher (0.40–0.57 wt%) than in the pyroxene-free inclusions (0.18–0.22 wt%).

Olivine in the spinel-pyroxene-olivine inclusions has a higher mean CaO content (0.84 ± 0.78 wt%) than olivine in the pyroxene-olivine inclusions (0.34 ± 0.02 wt%) (Table 4). However, the first standard deviation is so large that the differences in the mean CaO content of olivine between the two inclusion varieties may not be significant.

Phyllosilicate compositions are somewhat variable in the different varieties of inclusions. Mean phyllosilicate TiO_2 contents range from 0.12 to 0.55 wt%, mean Al_2O_3 contents range from 4.8 to 12.4 wt%, and mean CaO ranges from 0.61 to 2.5 wt%. The FeO content of phyllosilicate in the pyroxene inclusions and the spinel inclusions is moderately variable (±11 wt%) (Table 5). The mean FeO/MgO ratios in the inclusions vary from 2.6 to 3.6 (Table 5). If the phyllosilicate compositions are normalized to 100% and compared to those

Table 3. Mean compositions and standard deviations (wt%) of oxide phases in refractory inclusions in QUE 97990.

	Spinel-pyroxene inclusions		Spinel-pyroxene-olivine inclusions		Spinel inclusions		Hibonite-bearing inclusions	
	Spinel	Perovskite	Spinel	Perovskite	Spinel	Perovskite	Spinel	Hibonite
No. points	39	2	14	1	39	1	7	19
SiO_2	0.65 ± 1.1	0.37 ± 0.32	0.11 ± 0.10	<0.05	0.32 ± 0.39	0.09	0.19 ± 0.27	0.32 ± 0.13
TiO_2	0.34 ± 0.31	58.4 ± 1.1	0.19 ± 0.03	58.8	0.29 ± 0.16	57.6	0.29 ± 0.11	4.9 ± 0.9
Al_2O_3	69.5 ± 2.0	1.8 ± 0.7	70.2 ± 0.4	1.7	70.5 ± 0.9	2.1	70.4 ± 0.1	82.9 ± 1.3
Cr_2O_3	0.57 ± 0.78	<0.05	0.40 ± 0.19	<0.05	0.22 ± 0.06	<0.05	0.18 ± 0.07	0.05 ± 0.03
FeO	0.82 ± 0.47	0.84 ± 0.05	0.30 ± 0.11	0.17	0.84 ± 0.34	1.1	0.97 ± 0.26	0.76 ± 0.09
MnO	0.07 ± 0.08	<0.05	<0.05	<0.05	<0.05	<0.05	<0.05	<0.05
MgO	27.8 ± 0.7	0.56 ± 0.17	28.0 ± 0.2	0.84	28.0 ± 0.5	0.94	28.0 ± 0.1	2.9 ± 0.2
CaO	0.40 ± 0.57	40.2 ± 0.7	0.15 ± 0.08	39.8	0.39 ± 0.64	39.0	0.12 ± 0.05	8.3 ± 0.2
Total	100.2	102.2	99.4	101.3	100.6	100.8	100.2	100.1

The standard deviations reflect the spread in the mean compositions of the different refractory inclusions within each category.

in refractory inclusions in Cold Bokkeveld (Table 6 in Greenwood et al. 1994), it is clear that the QUE 97990 phyllosilicates are in the range of what Greenwood et al. (1994) labelled Mg-Fe serpentine.

Some inclusions contain patches of two distinct varieties of phyllosilicate. For example, hibonite-bearing inclusion F3r (Fig. 5a) contains phases that are mainly within the compositional ranges of the septechlorite minerals greenalite ($Fe_6Si_4O_{10}[OH]_8$) and chamosite ($[Fe_4Al_2][Si_2Al_2]O_{10}[OH]_8$). A phase (Table 6) that compositionally consists mainly of chamosite with minor amesite [another septechlorite mineral, $(Mg_4Al_2)(Si_2Al_2)O_{10}(OH)_8$] surrounds hibonite and spinel grains. A phase (Table 6) that compositionally consists of major greenalite and minor amesite and serpentine [$Mg_6Si_4O_{10}(OH)_8$] forms adjacent patches that typically do not enclose coarse grains of other minerals. The two distinct phyllosilicate phases in this single refractory inclusion probably formed by the alteration of different primary minerals.

DISCUSSION

Mineral Compositional Differences

Although the primary minerals in refractory inclusions may have formed by condensation, it is likely that typical nebular condensates were tiny (submicrometer) grains (e.g., Toppani et al. 2006) and that refractory-inclusion precursors were fluffy, porous dustballs (e.g., Blum and Schräpler 2004; Dominik and Tielens 1997). The relatively compact nature of the extant inclusions and the relatively coarse grain sizes of the constituent minerals reflect nebular processes involving appreciable melting of the inclusions and crystallization of the minerals (e.g., MacPherson and Davis 1993; Beckett et al. 2000; MacPherson et al. 2005). The minor differences in primary mineral compositions among the different varieties of refractory inclusions may be due in part to the inclusions' particular crystallization histories. It is also possible that there

Table 4. Mean compositions and standard deviations (wt%) of olivine in refractory inclusions in QUE 97990.

	Spinel-pyroxene-olivine inclusions	Pyroxene-olivine inclusions
No. points	15	14
SiO_2	42.8 ± 0.7	42.3 ± 0.4
TiO_2	<0.05	<0.05
Al_2O_3	0.06 ± 0.05	<0.05
Cr_2O_3	0.18 ± 0.14	0.15 ± 0.17
FeO	0.68 ± 0.61	0.65 ± 0.04
MnO	0.23 ± 0.27	0.22 ± 0.29
MgO	56.1 ± 1.3	57.2 ± 0.9
CaO	0.84 ± 0.78	0.34 ± 0.02
Total	100.9	100.9
Fa (mol%)	0.67 ± 0.61	0.63 ± 0.03

The standard deviations reflect the spread in the mean compositions of the different refractory inclusions within each category.

were some initial compositional differences among minerals in different types of refractory inclusions.

The essential absence of thermal metamorphic effects in CM chondrites (e.g., Grossman et al. 2005) and the presence of unaltered chondrule mafic-silicate phenocrysts in QUE 97990 (Rubin et al. 2007) suggest that there has been little cationic diffusion in coarse-grained minerals in this meteorite. Thus, the compositions of coarse oxide and silicate grains in QUE 97990 inclusions probably reflect primary igneous processes.

The spinel-pyroxene-olivine inclusions contain diopside with relatively high CaO and low FeO, and spinel with relatively low FeO (Table 2). Olivine in these inclusions has higher CaO than in the pyroxene-olivine inclusions. If spinel ($MgAl_2O_4$) crystallized first in these inclusions, the residual melt would become enriched in CaO, which could then partition into olivine and diopside. Because olivine crystallizes before diopside, olivine would incorporate FeO from the melt, leaving less of it available for the diopside. In olivine-free inclusion varieties, diopside would incorporate more FeO from the melt.

Table 5. Mean compositions and standard deviations (wt%) of phyllosilicate in refractory inclusions in QUE 97990.

	Spinel-pyroxene inclusions	Spinel-pyroxene-olivine inclusions	Pyroxene inclusions	Pyroxene-olivine inclusions	Spinel inclusions	Hibonite-bearing inclusions
No. points	11	2	13	1	8	6
SiO_2	21.2 ± 1.4	25.8 ± 2.1	24.7 ± 6.6	21.3	20.5 ± 6.6	20.9 ± 4.3
TiO_2	0.13 ± 0.06	0.44 ± 0.45	0.15 ± 0.10	0.43	0.12 ± 0.06	0.55 ± 0.37
Al_2O_3	5.8 ± 1.7	4.8 ± 2.4	4.9 ± 1.3	12.4	10.8 ± 15.3	11.3 ± 2.9
Cr_2O_3	0.05 ± 0.05	<0.04	0.11 ± 0.14	0.87	0.11 ± 0.09	<0.05
FeO	43.8 ± 3.3	39.5 ± 5.3	38.4 ± 11.1	37.7	36.9 ± 10.7	38.0 ± 3.6
MnO	0.18 ± 0.03	0.14 ± 0.06	0.19 ± 0.03	0.18	0.17 ± 0.07	0.17 ± 0.04
MgO	12.3 ± 1.6	13.2 ± 0.6	14.3 ± 5.5	14.7	12.6 ± 3.4	11.5 ± 0.9
CaO	0.65 ± 0.32	3.6 ± 4.5	0.61 ± 0.32	1.9	0.51 ± 0.35	2.5 ± 3.2
Na_2O	0.14 ± 0.05	0.10 ± 0.03	0.28 ± 0.22	0.10	0.27 ± 0.14	0.22 ± 0.07
K_2O	<0.05	<0.05	0.05 ± 0.05	<0.05	0.05 ± 0.05	<0.05
Total	84.2	87.6	83.7	89.6	82.0	85.1
FeO/MgO	3.6 ± 0.8	3.0 ± 0.3	2.7 ± 1.6	2.6	2.9 ± 1.5	3.3 ± 0.4

The standard deviations reflect the spread in the mean compositions of the different refractory inclusions within each category.

Table 6. Compositions (wt%) of two distinct phyllosilicate phases in hibonite-bearing inclusion F3r.

	Greenalite	Chamosite
No. points	1	1
SiO_2	17.5	16.2
TiO_2	0.07	0.18
Al_2O_3	5.1	22.3
Cr_2O_3	<0.05	0.07
FeO	46.4	32.6
MnO	0.16	0.17
MgO	10.7	15.9
CaO	0.84	0.17
Na_2O	0.31	0.11
K_2O	0.05	<0.05
Total	81.1	87.7
FeO/MgO	4.3	2.1

This discussion presupposes that some FeO was present in refractory inclusions prior to parent-body aqueous alteration or thermal metamorphism. This is supported by Russell et al. (1998), who reported that CO3.0 Colony contains Al-rich diopside with 0.21 wt% FeO in spinel-pyroxene inclusions, spinel with 0.5 wt% FeO in melilite-rich inclusions, and spinel with 0.39 wt% FeO in spinel-pyroxene inclusions. Colony has been severely affected by terrestrial weathering (Rubin et al. 1985) and it is possible that small limonite veins are responsible for the elevated FeO contents of some of the mineral phases. Nevertheless, the presence of hibonite-hercynite ($CaAl_{12}O_{19}$-$Fe^{+2}Al_2O_4$) inclusions in several CO3 chondrites, including Colony (Table 2 of Russell et al. 1998), indicates that some oxidized iron was present where and when these inclusions formed, prior to their incorporation into their parent body.

The variability in the compositions of phyllosilicate in the refractory inclusions probably reflects local conditions on the parent asteroid during aqueous alteration. Phyllosilicate composition is influenced by the initial porosity of a particular inclusion, compositions of the primary minerals, and local conditions of temperature, fluid composition, and water/rock ratio (e.g., Brearley 2006). Trigo-Rodríguez et al. (2006) inferred that local regions of relatively high porosity within CM chondrites exhibit stronger evidence of parent-body aqueous alteration.

Summary of CM Alteration

CM chondrites contain ~9 wt% indigenous water (Jarosewich 1990) bound in phyllosilicates formed during parent-body aqueous alteration (McSween 1979; Bunch and Chang 1980; Barber 1981; Tomeoka and Buseck 1985; Zolensky and Browning 1994; Zolensky et al. 1997; Browning et al. 2000; Trigo-Rodríguez et al. 2006). CM properties that change with progressive whole-rock alteration were explored by McSween (1979), Browning et al. (1996), and Hanowski and Brearley (2001).

The most recent scheme in classifying the degree of CM aqueous alteration is that of Rubin et al. (2007), who studied 11 CM chondrites that span the range from least altered to most altered. They used various petrologic properties (many previously identified) that provide information regarding the degree of aqueous alteration. Some properties result from processes associated with early and intermediate stages of the alteration sequence: hydration of matrix, alteration of primary igneous glass in chondrules, and production of large PCP clumps (i.e., serpentine-tochilinite intergrowths). Other petrologic properties reflect processes active throughout the alteration sequence; these include oxidation of metallic Fe-Ni, alteration of chondrule mafic phenocrysts, changes in PCP composition (reflecting an increase in the phyllosilicate/sulfide ratio), and changes in carbonate mineralogy (reflecting the development of dolomite and complex, Ca-, Mg-, Fe-, Mn-, and Ni-bearing carbonates at the expense of Ca carbonate).

Based on these parameters, Rubin et al. (2007) proposed a new aqueous alteration index for CM chondrites. Because there are no CM samples that display only incipient alteration, the least-altered sample was arbitrarily assigned to subtype 2.6. (One can infer from the experiments by Brearley and Burger [2007] on CO3 Kainsaz, which show the rapid onset of aqueous alteration at low temperatures, that unaltered CM chondrites are probably very rare and might not exist.) The most altered CM chondrites, currently classified CM1, were assigned to subtype 2.0. These rocks have essentially no mafic silicates; they contain chondrule pseudomorphs composed mainly of phyllosilicate.

The new alteration index follows historical precedent by assigning every CM chondrite to petrologic type 2. Lower numbers reflect higher degrees of alteration; this adheres to the scheme that type 1 carbonaceous chondrites are more altered than those of type 2 or 3. Finally, the closer the subtype is to type 3.0, the lesser the extent of whole-rock modification from its initial pristine state.

Petrologic subtypes were assigned to every CM chondrite in the Rubin et al. (2007) study: QUE 97990, CM2.6; Murchison, CM2.5; Kivesvaara, CM2.5; Murray, CM2.4/2.5; Y-791198, CM2.4; QUE 99355, CM2.3; Nogoya, CM2.2; Cold Bokkeveld, CM2.2; QUE 93005, CM2.1; LAP 02277, CM2.0; MET 01070, CM2.0.

Rarity of Melilite in CM Refractory Inclusions

There are only a few reported occurrences of melilite in CM refractory inclusions. Armstrong et al. (1982) reported a single anhedral melilite grain 1–2 μm in size enclosed within hibonite in the "Blue Angel" inclusion (1.5 mm in diameter) from CM2.5 Murchison. MacPherson et al. (1983) recovered a few melilite-rich inclusion fragments from Murchison derived from freeze-thaw disaggregation of the meteorite and heavy-liquid separations; these fragments may have been derived from a single disrupted melilite-rich inclusion. Melilite in portions of this inclusion is pitted with cavities produced by corrosion. MacPherson et al. (1983) also found blue spinel-hibonite spherules in Murchison containing small (≤20 μm) patches of melilite.

Simon et al. (2006) also used freeze-thaw methods to separate 40 spinel-rich inclusions from Murchison. Fifteen of these inclusions contain melilite: eight spinel-perovskite-melilite inclusions, six spinel-hibonite-perovskite-melilite inclusions, and one spinel-melilite-anorthite inclusion. Both coarse- and fine-grained melilite grains occur in the inclusions.

Freeze-thaw disaggregation of CM2 Lewis Cliff (LEW) 85311 yielded a few spinel-hibonite-melilite inclusions (Simon et al. 2005). This meteorite was chosen because its ^{16}O-rich bulk oxygen-isotopic composition ($\Delta^{17}O = -3.23‰$; Clayton and Mayeda 1999) suggested a low degree of aqueous alteration (cf. Fig. 8 of Rubin et al. 2007).

Destruction of Melilite During Aqueous Alteration

The most primitive carbonaceous chondrites contain abundant melilite-rich refractory inclusions. The Acfer 094 ungrouped (CM-related) type 3.0 carbonaceous chondrite contains refractory inclusions rich in melilite and spinel (Weber 1995). Russell et al. (1998) found that ~45% of the refractory inclusions in the least-altered (type 3.0) CO chondrites are melilite-rich. This percentage is probably an underestimate because the two CO3.0 chondrites (Colony and ALHA77307) that Russell et al. investigated have experienced significant terrestrial weathering, a process that could have caused the degradation of some refractory inclusions. A less-weathered CO3.0 chondrite is Y-81020. Kojima et al. (1995) identified 27 refractory inclusions (excluding amoeboid olivine inclusions) in Y-81020; twenty of these inclusions (i.e., 74%) are rimmed objects rich in spinel, pyroxene, and melilite.

CR chondrites possess abundant metallic Fe-Ni and several rocks contain chondrules with unaltered (or only slightly altered) glassy mesostases. Although these rocks have undergone aqueous alteration, most alteration effects are confined to the fine-grained serpentine- and saponite-rich matrix (Brearley 2006). Approximately half of the refractory inclusions in CR2 chondrites are melilite-rich (Weisberg et al. 1993; Weber and Bischoff 1997).

Hydrothermal experiments show that gehlenite (the main component of melilite in the majority of refractory inclusions) (Brearley and Jones 1998) is highly susceptible to alteration (Nomura and Miyamoto 1998). Compared to other common phases in refractory inclusions, melilite breaks down more rapidly into secondary products.

In those CO3 chondrites (e.g., CO3.5 Lancé) that have experienced intermediate degrees of fluid-assisted metamorphism or hydrothermal-alteration/thermal-metamorphism (e.g., McSween 1977; Rubin 1998), melilite is replaced by feldspathoids, diopside, and sulfide (Russell et al. 1998). In a survey of refractory inclusions in the Moss CO3.5/3.6 chondrite fall, Bischoff and Schmale (2007) found only a single (altered) melilite-bearing inclusion. In the most metamorphosed CO3 chondrites (e.g., CO3.7 Warrenton and CO3.8 Isna), none of the inclusions contains melilite (Russell et al. 1998).

This trend of melilite disappearance with increasing degree of whole-rock alteration is also evident among refractory inclusions in CV3 chondrites. Oxidized CV meteorites such as Allende (which have experienced appreciable whole-rock aqueous alteration) (Krot et al. 1995) contain fluffy type A inclusions wherein most of the primary melilite has been replaced by fine-grained secondary alteration products (anorthite, nepheline, grossular, and sodalite) (MacPherson and Grossman 1984). Reduced CV meteorites such as Vigarano, which have experienced appreciably less whole-rock alteration, contain essentially unaltered melilite (MacPherson and Grossman 1984).

Modal Abundances and Number Densities of Refractory Inclusions

Although aqueous alteration of carbonaceous chondrites is not a high-energy process (Hanowski and Brearley 2000), it does appear to cause some refractory inclusions to fragment and disintegrate (e.g., Armstrong et al. 1982).

QUE 97990 (type 2.6) contains 1.8 vol% refractory inclusions. The 40 inclusions identified within an area of ~0.5 cm^2 indicate a number density of ~80 inclusions/cm^2. Because 65% of the inclusions are largely intact, the number density of largely intact inclusions is ~50 inclusions/cm^2.

The mineralogical alteration index of Browning et al. (1996) places Mighei about halfway between Nogoya and Murray. Because these two meteorites were classified by Rubin et al. (2007) as type 2.2 and 2.4/2.5, respectively, Mighei is probably around type 2.3. This classification is consistent with the observation of MacPherson and Davis (1994) that refractory inclusions in Mighei "seem to be more altered than those in Murray (type 2.4/2.5) and Murchison (type 2.5)." MacPherson and Davis (1994) reported a total of 35 refractory inclusions in three thin sections of Mighei. They determined that Mighei contains ~10 inclusions/cm^2. This implies that the surface area of the thin sections totalled ~3.5 cm^2. Although the MacPherson-Davis inventory was not meant to be comprehensive, a very rough estimate of the modal abundance of inclusions can be made. From the sizes of the individual inclusions listed in Table 1 of MacPherson and Davis (1994), I calculate that the modal abundance of refractory inclusions in Mighei is ~0.6 vol%. However, 47% of the total surface area of the refractory inclusions is contained within one large (600 × 1700 μm) spinel-pyroxene inclusion (#1–21); if this single inclusion were omitted from the set, the approximate number density would not change, but the modal abundance of inclusions in Mighei would drop to ~0.3 vol%.

Cold Bokkeveld (type 2.2) has a number density of ~60 refractory inclusions/cm^2 (Greenwood et al. 1994), but almost all of these are fragments of larger disrupted objects. If 10% of the refractory inclusions are largely intact (probably an overestimate), then the number density of such inclusions in Cold Bokkeveld is on the order of 6 inclusions/cm^2.

To calculate the modal abundance of refractory inclusions in Cold Bokkeveld, I used the proportions and size ranges of the different varieties of inclusions (Table 3a in Greenwood et al. 1994), and assumed (without evidence but for the sake of simplicity) that the inclusions were equant and that the mean size of each variety was in the middle of its size range. From these values and the total thin section surface area of 588 mm^2 (Table 1 in Greenwood et al. 1994), I derive a modal abundance of ~0.01 vol% refractory inclusions.

These data show correlations in CM chondrites between petrologic subtype and modal abundance and between petrologic subtype and number density of largely intact refractory inclusions. It is apparent that parent-body aqueous processes altered refractory inclusions, causing them to disrupt. CM chondrites that have experienced greater degrees of aqueous alteration have lower modal abundances and lower number densities of refractory inclusions. Although data on additional CM chondrites is required, it seems plausible that these parameters will prove useful indicators for tracking progressive whole-rock alteration of CM chondrites.

Fragmentation of altered refractory inclusions is also consistent with the observations that 1) the smallest spinel-bearing inclusions are the spinel inclusions (which consist essentially of spinel and phyllosilicate), 2) these inclusions are all fragments, and 3) these inclusions have the highest mean modal abundance of phyllosilicates (~50 vol%) of any inclusion type.

The process of melilite alteration also occurred in CO3 chondrites. The fine-grained refractory inclusions in CO3 chondrites may have formed by the breakdown of melilite-rich inclusions during hydrothermal-alteration/thermal-metamorphism (Russell et al. 1998). The data in Table 2 in Russell et al. show that if the fine-grained inclusions are excluded from consideration, then the number density of refractory inclusions in CO3 chondrites tends to decrease with increasing degrees of whole-rock alteration (using the subtypes recommended by Chizmadia et al. 2002): CO3.0 ALHA77307 contains 0.28 inclusions/mm^2; CO3.5 Lancé contains 0.24 inclusions/mm^2; CO3.7 Warrenton and CO3.8 Isna each contain 0.16 inclusions/mm^2. These data show a strong anti-correlation between petrologic subtype and number density: $r = -0.99$, $n = 4$, $2\alpha = 0.01$, significant at the 99% confidence level.

Origin of Spinel Inclusions

Equilibrium thermodynamic calculations show that spinel condenses at lower temperatures than gehlenitic melilite from a gas of solar composition (e.g., Grossman 1972; Lattimer and Grossman 1978; Wood and Hashimoto 1993; Yoneda and Grossman 1995). Thus, under normal circumstances, spinel-bearing inclusions would be expected to also contain melilite.

Several workers have formulated complex nebular models in attempts to account for the occurrence of melilite-free spinel inclusions in CM chondrites. MacPherson and Davis (1994) invoked a vague process involving "some kind of nebular condensation combined with aggregation." Beckett and Stolper (1994) suggested that spinel may have nucleated directly upon hibonite and that condensation of melilite was suppressed because the gas was depleted in Al. It is also possible that disequilibrium condensation of supercooled nebular gas caused spinel to nucleate prior to melilite (Wood 2004; Petaev et al. 2005). Simon et al. (2006) suggested that melilite condensation was kinetically inhibited and that spinel condensed preferentially.

Because melilite does not seem to have been a significant precursor phase of Al-rich chondrules in ordinary chondrites, MacPherson and Huss (2005) suggested that melilite-rich inclusions were separated in the nebula from inclusions that were essentially free of melilite. The melilite-rich inclusions were sequestered in an environment where they could not react further with nebular gas (possibly by having been entrained in bipolar outflows) (Shu et al. 1996). After chondrule formation, the melilite-rich inclusions were reintroduced into the chondrite agglomeration zone. An analogous separation of refractory inclusions on the basis of melilite content in the CM region could conceivably account for the virtual absence of melilite-bearing inclusions in CM chondrites if they were not reintroduced into the CM agglomeration zone. It is unclear, however, how refractory inclusions could be separated on the basis of their melilite content or what mechanisms could account for the sequestration of melilite-rich inclusions in the nebula or, in some cases, their introduction to chondrite agglomeration zones.

Cohen (1981), Cohen et al. (1983), and Kornacki and Fegley (1984) explored unusual inclusion-melting scenarios. They proposed that melilite-free inclusions formed by a process involving loss of melt from partially molten inclusions that contained solid grains consisting solely of spinel.

I reject all of these models. It seems more likely that melilite-free spinel inclusions in CM chondrites formed by parent-body aqueous alteration and disaggregation of melilite-bearing inclusions. The process involved alteration of primary melilite (thereby enhancing inclusion friability) and subsequent fragmentation of the inclusions; in many cases, other phases (e.g., olivine, pyroxene, hibonite) were dislodged from the inclusions and separated from the spinel. Because melilite is typically associated with spinel in refractory inclusions in primitive carbonaceous chondrites (e.g., CO3.0 Colony, ALHA77307, and Y-81020) (Russell et al. 1998; Kojima et al. 1995), this model is consistent with the fragmental nature of all of the spinel inclusions in QUE 97990 (Table 1; Fig. 2) and the occurrence of high amounts of phyllosilicate in these inclusions. The phyllosilicates probably formed on the parent asteroid mainly by alteration of melilite. This is consistent with the textural resemblance of some phyllosilicate-bearing spinel-pyroxene inclusions in CM2.6 QUE 97990 to some spinel-pyroxene-melilite inclusions in CO3.0 Y-81020 (banded inclusions G6v and E8y to Y20-41 [Fig. 1 in Kojima et al. 1995] and nodular inclusion E2u to Y20-16 [Fig. 2 of Kojima et al. 1995]).

Furthermore, there are no plausible phases other than melilite that could have been present in abundance in the original unaltered spinel and spinel-pyroxene inclusions in QUE 97990 that could have been entirely replaced by phyllosilicate.

In CO3 chondrites, the proportion of refractory inclusions containing spinel and pyroxene (but no other principal phases) increases with metamorphic subtype. For example, spinel-pyroxene inclusions constitute 42–47% of all refractory inclusions in type 3.0 ALHA77307 and type 3.0 Colony, and 94% of the inclusions in type 3.8 Isna (Russell et al. 1998) (using the CO3 subtype designations of Chizmadia et al. 2002). It seems plausible that many of the spinel-pyroxene inclusions in the more-metamorphosed CO3 chondrites formed from spinel-pyroxene-melilite inclusions with increasing whole-rock alteration resulting in the progressive destruction of melilite.

Although melilite in refractory inclusions is replaced in part by feldspathoids in metamorphosed CO3 chondrites and oxidized CV3 chondrites (e.g., Russell et al. 1998; MacPherson and Grossman 1984), such phases have not been observed in CM refractory inclusions. This does not mean, however, that melilite has not been altered in CM inclusions. CM chondrites experienced extensive aqueous alteration with little accompanying thermal metamorphism (e.g., McSween 1979, 1987; Bunch and Chang 1980; Tomeoka and Buseck 1985; Zolensky and Browning 1994; Zolensky et al. 1997; Browning et al. 1996, 2000; Hanowski and Brearley 2001; Chizmadia and Brearley 2003, 2004; Rubin et al. 2007). Under these conditions, melilite altered directly to phyllosilicate. The CM-chondrite style of alteration is different than that undergone by CO chondrites (which experienced fluid-assisted thermal metamorphism; e.g., McSween 1977; Scott and Jones 1990; Rubin 1998; Brearley 2006) or CV chondrites (which experienced oxidation and aqueous metasomatism; e.g., Krot et al. 1995, 1998a, 1998b, 2000; Brearley 1999).

CONCLUSIONS

The most abundant refractory inclusions in QUE 97990 consist (in addition to phyllosilicate) mainly of spinel-pyroxene (35%), followed by those composed primarily of spinel (20%), spinel-pyroxene-olivine (18%), pyroxene (12%), pyroxene-olivine (8%), and hibonite ± spinel (8%). Four pyroxene phases occur: diopside, Al-rich diopside, Al-Ti diopside (fassaite), and, in two inclusions, enstatite. No inclusions contain melilite.

Whole-rock aqueous alteration of carbonaceous chondrites causes refractory inclusions to break apart. The least-altered CM chondrite (QUE 97990; CM2.6) contains the highest modal abundance and highest number density of refractory inclusions: 1.8 vol% inclusions (~50 largely intact inclusions/cm^2). More-altered CM chondrites have lower modal abundances and lower number densities of refractory inclusions: literature data imply that Mighei (CM ~ 2.3) contains roughly 0.3–0.6 vol% inclusions (~10 largely intact inclusions/cm^2) and Cold Bokkeveld (CM2.2) contains ~0.01 vol% inclusions (on the order of 6 largely intact inclusions/cm^2).

Melilite-free, phyllosilicate-rich, spinel. and spinel-pyroxene inclusions in CM chondrites formed from pristine, phyllosilicate-free, melilite-bearing inclusions by aqueous alteration of melilite on the parent asteroid. This increased inclusion friability. Alteration was accompanied or followed by fragmentation and disaggregation of many inclusions. In some cases, other phases (e.g., olivine, pyroxene, hibonite) in the inclusions were dislodged and separated from the spinel.

Editorial Handling—Dr. Christine Floss

REFERENCES

Armstrong J. T., Meeker G. P., Huneke J. C., and Wasserburg G. J. 1982. The Blue Angel: I. The mineralogy and petrology of a hibonite inclusion from the Murchison meteorite. *Geochimica et Cosmochimica Acta* 46:575–595.

Barber D. J. 1981. Matrix phyllosilicates and associated minerals in C2M carbonaceous chondrites. *Geochimica et Cosmochimica Acta* 45:945–970.

Barber D. J. 1985. Phyllosilicates and other layer-structured materials in stony meteorites. *Clay Mineralogy* 20:415–454.

Beckett J. R. and Stolper E. 1994. The stability of hibonite, melilite, and other aluminous phases in silicate melts: Implications for the origin of hibonite-bearing inclusions from carbonaceous chondrites. *Meteoritics* 29:41–65.

Beckett J. R., Simon S. B., and Stolper E. 2000. The partitioning of Na between melilite and liquid: Part II. Applications to type B inclusions from carbonaceous chondrites. *Geochimica et Cosmochimica Acta* 64:2519–2534.

Bischoff A. and Schmale K. 2007. Ca,Al-rich inclusions within the Moss CO3 chondrite—Indications for severe secondary alteration (abstract #1561). 38th Lunar and Planetary Science Conference. CD-ROM.

Blum J. and Schräpler R. 2004. Structure and mechanical properties of high-porosity macroscopic agglomerates formed by random ballistic deposition. *Physical Review Letters* 93:115503-1–115503-4.

Brearley A. J. 1999. Origin of graphitic carbon and pentlandite inclusions in matrix olivines in the Allende meteorite. *Science* 285:1380–1382.

Brearley A. J. 2006. The action of water. In *Meteorites and the early solar system II*, edited by Lauretta D. S. and McSween H. Y. Jr. Tucson, Arizona: The University of Arizona Press. pp. 587–624.

Brearley A. J. and Burger P. V. 2007. Hydrothermal alteration behavior of Kainsaz (CO3) at low temperatures under reducing conditions: Insights into incipient aqueous alteration of carbonaceous chondrites (abstract #1687). 38th Lunar and Planetary Science Conference. CD-ROM.

Brearley A. J. and Jones R. H. 1998. Chondritic meteorites. In *Planetary materials*, edited by Papike J. J. Reviews in Mineralogy vol. 36. Washington, D.C.: Mineralogical Society of America. pp. 3-1–3-398.

Browning L., McSween H. Y. Jr., and Zolensky M. 1996. Correlated alteration effects in CM carbonaceous chondrites. *Geochimica et Cosmochimica Acta* 60:2621–2633.

Browning L., McSween H. Y. Jr., and Zolensky M. E. 2000. On the origin of rim textures surrounding anhydrous silicate grains in CM carbonaceous chondrites. *Meteoritics & Planetary Science* 35:1015–1023.

Bunch T. and Chang S. 1980. Carbonaceous chondrites—II. Carbonaceous chondrite phyllosilicates and light element geochemistry as indicators of parent body processes and surface conditions. *Geochimica et Cosmochimica Acta* 44:1543–1577.

Chizmadia L. J. and Brearley A. J. 2003. Mineralogy and textural characteristics of fine-grained rims in the Yamato-791198 CM2 carbonaceous chondrite: Constraints on the location of aqueous alteration (abstract #1419). 34th Lunar and Planetary Science Conference. CD-ROM.

Chizmadia L. J. and Brearley A. J. 2004. Aqueous alteration of carbonaceous chondrites: New insights from comparative studies of two unbrecciated CM2 chondrites, Y-791198 and ALH 81002 (abstract #1753). 35th Lunar and Planetary Science Conference. CD-ROM.

Chizmadia L. J., Rubin A. E., and Wasson J. T. 2002. Mineralogy and petrology of amoeboid olivine inclusions in CO3 chondrites: Relationship to parent-body aqueous alteration. *Meteoritics & Planetary Science* 37:1781–1796.

Clayton R. N. and Mayeda T. K. 1999. Oxygen isotope studies of carbonaceous chondrites. *Geochimica et Cosmochimica Acta* 63: 2089–2104.

Cohen R. E. 1981. Refractory inclusions in the Mokoia C3(V) carbonaceous chondrite (abstract). *Meteoritics* 16:304.

Cohen R. E., Kornacki A. S. and Wood J. A. 1983. Mineralogy and petrology of chondrules and inclusions in the Mokoia CV3 chondrite. *Geochimica et Cosmochimica Acta* 47:1739–1757.

Dominik C. and Tielens A. G. G. M. 1997. The physics of dust coagulation and the structure of dust aggregates in space. *The Astrophysical Journal* 480:647–673.

Ford R. and Brearley A. J. 2007. Phyllosilicates in two coarse-grained Allende CAIs: Evidence for advanced hydration (abstract #2411). 38th Lunar and Planetary Science Conference. CD-ROM.

Fuchs L. H., Olsen E., and Jensen K. J. 1973. Mineralogy, mineral-chemistry, and composition of the Murchsion (C2) meteorite. *Smithsonian Contributions to the Earth Sciences* 10:1–39.

Greenwood R. C., Lee M. R., Hutchison R., and Barber D. J. 1994. Formation and alteration of CAIs in Cold Bokkeveld (CM2). *Geochimica et Cosmochimica Acta* 58:1913–1935.

Grossman J. N., Zolensky M. E., and Tonui E. K. 2005. What are the petrologic types of thermally metamorphosed CM chondrites? (abstract) *Meteoritics & Planetary Science* 40:A61.

Grossman L. 1972. Condensation in the primitive solar nebula. *Geochimica et Cosmochimica Acta* 36:597–619.

Hanowski N. P. and Brearley A. J. 2000. Iron-rich aureoles in the CM carbonaceous chondrites Murray, Murchison, and Allan Hills 81002: Evidence for in situ aqueous alteration. *Meteoritics & Planetary Science* 35:1291–1308.

Hanowski N. P. and Brearley A. J. 2001. Aqueous alteration of chondrules in the CM carbonaceous chondrite, Allan Hills 81002: Implications for parent body alteration. *Geochimica et Cosmochimica Acta* 65:495–518.

Jarosewich E. 1990. Chemical analyses of meteorites: A compilation of stony and iron meteorite analyses. *Meteoritics* 25:323–337.

Kojima T., Yada S., and Tomeoka K. 1995. Ca-Al-rich inclusions in three Antarctic CO3 chondrites, Yamato-81020, Yamato-82050, and Yamato-790992: Record of low-temperature alteration. *Proceedings of the NIPR Symposium on Antarctic Meteorite*s 8: 79–96.

Kornacki A. S. and Fegley B. 1984. Origin of spinel-rich chondrules and inclusions in carbonaceous and ordinary chondrites. *Journal of Geophysical Research* 89:B588–B596.

Krot A. N., Scott E. R. D., and Zolensky M. E. 1995. Mineralogical and chemical modification of components in CV3 chondrites: Nebular or asteroidal processing? *Meteoritics* 30:748–775.

Krot A. N., Petaev M. I., Zolensky M. E., Keil K., Scott E. R. D., and Nakamura K. 1998a. Secondary calcium-iron-rich minerals in the Bali-like and Allende-like oxidized CV3 chondrites and Allende dark inclusions. *Meteoritics & Planetary Science* 33: 623–645.

Krot A. N., Petaev M. I., Scott E. R. D., Choi B.-G., Zolensky M. E. and Keil K. 1998b. Progressive alteration in CV3 chondrites: More evidence for asteroidal alteration. *Meteoritics & Planetary Science* 33:1065–1085.

Krot A. N., Petaev M. I., Meibom A., and Keil K. 2000. In situ growth of Ca-rich rims around Allende dark inclusions. *Geochemistry International* 38:S351–S368.

Kunihiro T., Rubin A. E., and Wasson J. T. 2005. Oxygen-isotopic compositions of low-FeO relics in high-FeO host chondrules in Acfer 094, a type 3.0 carbonaceous chondrite closely related to CM. *Geochimica et Cosmochimica Acta* 69:3831–3840.

Lattimer J. M. and Grossman L. 1978. Chemical condensation sequences in supernova ejecta. *The Moon and the Planets* 19: 169–184.

Macdougall J. D. 1979. Refractory-element-rich inclusions in CM meteorites. *Earth and Planetary Science Letters* 42:1–6.

Macdougall J. D. 1981. Refractory spherules in the Murchison meteorite: Are they chondrules? *Geophysical Research Letters* 8: 966–969.

MacPherson G. J. and Davis A. M. 1993. A petrologic and ion microprobe study of a Vigarano type B2 refractory inclusion: Evolution by multiple stages of melting and alteration. *Geochimica et Cosmochimica Acta* 57:231–243.

MacPherson G. J. and Davis A. M. 1994. Refractory inclusions in the prototypical CM chondrite Mighei. *Geochimica et Cosmochimica Acta* 58:5599–5625.

MacPherson G. J. and Grossman L. 1984. "Fluffy" type A Ca,Al-rich inclusions in the Allende meteorite. *Geochimica et Cosmochimica Acta* 48:29–46.

MacPherson G. J. and Huss G. R. 2005. Petrogenesis of Al-rich chondrules: Evidence from bulk compositions and phase equilibria. *Geochimica et Cosmochimica Acta* 69:3099–3127.

MacPherson G. J., Bar-Matthews M., Tanaka T., Olsen E., and Grossman L. 1983. Refractory inclusions in the Murchison meteorite. *Geochimica et Cosmochimica Acta* 47:823–839.

MacPherson G. J., Simon S. B., Davis A. M., Grossman L., and Krot A. N. 2005. Calcium-aluminum-rich inclusions: Major unanswered questions. In *Chondrites and the protoplanetary disk*, edited by Krot A. N., Scott E. R. D., and Reipurth B. ASP Conference Series #341. San Francisco: Astronomical Society of the Pacific. pp. 225–250.

McSween H. Y. Jr. 1977. Carbonaceous chondrites of the Ornans type: A metamorphic sequence. *Geochimica et Cosmochimica Acta* 41:477–491.

McSween H. Y. Jr. 1979. Alteration in CM carbonaceous chondrites inferred from modal and chemical variations in matrix. *Geochimica et Cosmochimica Acta* 43:1761–1770.

McSween H. Y. Jr. 1987. Aqueous alteration in carbonaceous chondrites: mass balance constraints on matrix mineralogy. *Geochimica et Cosmochimica Acta* 51:2469–2477.

Newton J., Bischoff A., Arden J. W., Franchi I. A., Geiger T., Greshake A., and Pillinger C. T. 1995. Acfer 094, a uniquely primitive carbonaceous chondrite from the Sahara. *Meteoritics* 30:47–56.

Nomura K. and Miyamoto M. 1998. Hydrothermal experiments on alteration of Ca-Al-rich inclusions (CAIs) in carbonaceous chondrites: Implications for aqueous alteration in parent asteroids. *Geochimica et Cosmochimica Acta* 62:3575–3588.

Petaev M. I., Krot A. N., and Wood J. A. 2005. Nebular condensation under incomplete equilibrium: Implications for the fine-grained spinel-rich CAIs (abstract #1238). 36th Lunar and Planetary Science Conference. CD-ROM.

Rubin A. E. 1998. Correlated petrologic and geochemical characteristics of CO3 chondrites. *Meteoritics & Planetary Science* 33:385–391.

Rubin A. E. and Kallemeyn G. W. 1990. Lewis Cliff 85332: A unique carbonaceous chondrite. *Meteoritics* 25:215–225.

Rubin A. E., James J. A., Keck B. D., Weeks K. S., Sears D. W. G., and Jarosewich E. 1985. The Colony meteorite and variations in CO3 chondrite properties. *Meteoritics* 20:175–196.

Rubin A. E., Trigo-Rodríguez J. M., Huber H., and Wasson J. T. 2007. Progressive aqueous alteration of CM carbonaceous chondrites. *Geochimica et Cosmochimica Acta* 71:2361–2382.

Russell S. S., Huss G. R., Fahey A. J., Greenwood R. C., Hutchison R., and Wasserburg G. J. 1998. An isotopic and petrologic study of calcium-aluminum-rich inclusions from CO3 meteorites. *Geochimica et Cosmochimica Acta* 62:689–714.

Scott E. R. D. and Jones R. H. 1990. Disentangling nebular and asteroidal features of CO3 carbonaceous chondrite meteorites. *Geochimica et Cosmochimica Acta* 54:2485–2502.

Shu F. H., Shang H., and Lee T. 1996. Toward an astrophysical theory of chondrites. *Science* 271:1545–1552.

Simon S. B., Keaton C. G. and Grossman L. 2005. Refractory inclusions from the CM2 chondrite LEW 85311 (abstract). *Meteoritics & Planetary Science* 40:A141.

Simon S. B., Grossman L., Hutcheon I. D., Phinney D. L., Weber P. K., and Fallon S. J. 2006. Formation of spinel-, hibonite-rich inclusions found in CM2 carbonaceous chondrites. *American Mineralogist* 91:1675–1687.

Tomeoka K. and Buseck P. R. 1985. Indicators of aqueous alteration in CM carbonaceous chondrites: Microtextures of a layered mineral containing Fe, S, O, and Ni. *Geochimica et Cosmochimica Acta* 49:2149–2163.

Toppani A., Libourel G., Robert F., and Ghanbaja J. 2006. Laboratory condensation of refractory dust in protosolar and circumstellar conditions. *Geochimica et Cosmochimica Acta* 70:5035–5060.

Trigo-Rodríguez J. M., Rubin A. E., and Wasson J. T. 2006. Non-nebular origin of dark mantles around chondrules and inclusions in CM chondrites. *Geochimica et Cosmochimica Acta* 70:1271–1290.

Weber D. 1995. Refractory inclusions from the carbonaceous chondrite Acfer 094 (abstract). *Meteoritics* 30:595–596.

Weber W. and Bischoff A. 1997. Refractory inclusions in the CR chondrite Acfer 059-El Djouf 001: Petrology, chemical composition, and relationship to inclusion populations in other types of carbonaceous chondrites. *Chemie der Erde* 57:1–24.

Weisberg M. K., Prinz M., Clayton R. N., and Mayeda T. K. 1993. The CR (Renazzo-type) carbonaceous chondrite group and its implications. *Geochimica et Cosmochimica Acta* 57:1567–1586.

Wood J. A. 2004. Formation of chondritic refractory inclusions: The astrophysical setting. *Geochimica et Cosmochimica Acta* 68: 4007–4021.

Wood J. A. and Hashimoto A. 1993. Mineral equilibrium in fractionated nebular systems. *Geochimica et Cosmochimica Acta* 57:2377–2388.

Yoneda S. and Grossman L. 1995. Condensation of CaO-MgO-Al_2O_3-SiO_2 liquids from cosmic gases. *Geochimica et Cosmochimica Acta* 59:3413–3444.

Zolensky M. and Browning L. 1994. CM chondrites exhibit the complete petrologic range from type 2 to 1 (abstract). *Meteoritics* 29:556.

Zolensky M. E., Mittlefehldt D. W., Lipschutz M. E., Wang M.-S., Clayton R. N., Mayeda T. K., Grady M. M., Pillinger C. T., and Barber D. 1997. CM chondrites exhibit the complete petrologic range from type 2 to 1. *Geochimica et Cosmochimica Acta* 61: 5099–5115.